Muscle-Specific Vascular Endothelial Growth Factor Deletion Induces Muscle Capillary Rarefaction Creating Muscle Insulin Resistance

Jeffrey S. Bonner,[1] Louise Lantier,[1] Clinton M. Hasenour,[1] Freyja D. James,[1] Deanna P. Bracy,[1,2] and David H. Wasserman[1,2]

Muscle insulin resistance is associated with a reduction in vascular endothelial growth factor (VEGF) action and muscle capillary density. We tested the hypothesis that muscle capillary rarefaction critically contributes to the etiology of muscle insulin resistance in chow-fed mice with skeletal and cardiac muscle VEGF deletion ($mVEGF^{-/-}$) and wild-type littermates ($mVEGF^{+/+}$) on a C57BL/6 background. The $mVEGF^{-/-}$ mice had an ~60% and ~50% decrease in capillaries in skeletal and cardiac muscle, respectively. The $mVEGF^{-/-}$ mice had augmented fasting glucose turnover. Insulin-stimulated whole-body glucose disappearance was blunted in $mVEGF^{-/-}$ mice. The reduced peripheral glucose utilization during insulin stimulation was due to diminished in vivo cardiac and skeletal muscle insulin action and signaling. The decreased insulin-stimulated muscle glucose uptake was independent of defects in insulin action at the myocyte, suggesting that the impairment in insulin-stimulated muscle glucose uptake was due to poor muscle perfusion. The deletion of VEGF in cardiac muscle did not affect cardiac output. These studies emphasize the importance for novel therapeutic approaches that target the vasculature in the treatment of insulin-resistant muscle. ***Diabetes*** **62:572–580, 2013**

Insulin resistance is closely associated with cardiovascular disease and together they are central to the metabolic syndrome (1). Skeletal muscle contributes ~80% of insulin-mediated glucose disposal, thus impairments in insulin-stimulated muscle glucose uptake (MGU) are critical to the pathogenesis of insulin resistance. Pharmacologically limiting glucose and insulin delivery to the muscle impairs insulin-stimulated MGU (2); moreover, reduced blood flow to the muscle is correlated with insulin resistance (3–6). Recent studies have linked diet-induced extramyocellular adaptations to insulin resistance in rodent models (7–9) and humans (10). The number of capillaries perfusing the muscle is positively related to peripheral insulin action, independent of age, body composition, energy expenditure, and lipid status (11). The important question that remains to be answered is whether the reduction in capillaries is a cause or consequence of muscle insulin resistance.

From the [1]Department of Molecular Physiology and Biophysics, Vanderbilt University School of Medicine, Nashville, Tennessee; and the [2]Mouse Metabolic Phenotyping Center, Vanderbilt University School of Medicine, Nashville, Tennessee.
Corresponding author: Jeffrey S. Bonner, jeffrey.s.bonner@vanderbilt.edu.
Received 20 March 2012 and accepted 20 July 2012.
DOI: 10.2337/db12-0354

See accompanying commentary, p. 343.

Insulin recruits unperfused capillaries, which enhances nutrient blood flow to metabolically active muscle. The augmented microvascular blood volume precedes insulin-stimulated MGU (12). Studies estimate that 40% of insulin-stimulated MGU results from increased muscle perfusion and that this hemodynamic response is absent in patients with type 2 diabetes (2,6,13–17). Muscle capillarity is an important predictor of insulin-mediated glucose disposal, and accordingly, insulin-resistant humans and rodents exhibit capillary rarefaction (9,18–21). Pharmacological agents that target the vasculature to increase tissue perfusion also improve skeletal muscle insulin resistance and augment muscle microvascular density (7,9,22). This affirms the importance of restoring skeletal muscle perfusion in ameliorating insulin resistance (7,9,22,23).

The vascular endothelial growth factor (VEGF) family of proteins regulates vasculogenesis, angiogenesis, and lymphanogenesis (24). In particular, VEGF-A stimulates the formation of new vascular networks by recruiting and differentiating endothelial progenitor cells in addition to inducing endothelial cell proliferation and migration (24). Insulin-resistant states are characterized by impaired VEGF-A action in the vascular beds of cardiac and skeletal muscle triggering capillary regression (18,25–27). Cardiac and skeletal myocellular VEGF-A production regulates capillarity by paracrine signaling to the endothelium (28,29). Capillary density correlates with the severity of insulin resistance in obesity; however, the specific effect of capillary rarefaction to the pathogenesis of skeletal and cardiac muscle insulin resistance has not been elucidated (8,9,11,19).

The experiments described herein test the hypothesis that skeletal and cardiac muscle capillary rarefaction in lean, otherwise healthy mice impairs muscle insulin action. Genetic deletion of skeletal and cardiac muscle *VEGF-A* (subsequently referred to as VEGF) was used to selectively reduce muscle capillarity in lean mice to determine the specific consequence of capillary rarefaction on insulin-stimulated MGU.

RESEARCH DESIGN AND METHODS

Murine models. The Vanderbilt University Animal Care and Use Committee approved all animal protocols. Mice were housed with a 12:12-h light–dark cycle in a temperature- and humidity-controlled environment. Mice were fed a chow diet (5.5% fat by weight; 5001 Purina Laboratory Rodent Diet) for 9 weeks beginning at age 3 weeks, and all studies were performed at age 12 weeks. Mice with a muscle-specific genetic deletion of *VEGF* were studied. Mice with LoxP sites flanking exon 3 of the *VEGF* gene on a congenic background (30) and mice expressing Cre recombinase under the muscle creatine kinase (*MCK*) promoter (purchased from Jackson Laboratory) were crossed to generate the MCK-cre/$VEGF^{lox/lox}$ ($mVEGF^{-/-}$) mice and wild-type littermates $VEGF^{lox/lox}$ ($mVEGF^{+/+}$). Mice were backcrossed on to a C57BL/6 background for at least 10 generations. The *MCK* promoter is expressed in

skeletal and cardiac muscle. *mVEGF*$^{-/-}$ mice lack all VEGF-A isoforms from skeletal and cardiac muscle. Genotyping was performed as previously described (28).

Assessment of body composition and cardiac function. Body composition was determined using an mq10 nuclear magnetic resonance analyzer (Bruker Optics). Echocardiogram (Sonos 5500 system; Agilent) was used to assess cardiac output, and blood pressure was measured with a blood pressure transducer via a carotid arterial catheter with the assistance of the Cardiovascular Pathophysiology and Complications Core of the Vanderbilt Mouse Metabolic Phenotyping Center (VMMPC).

Hyperinsulinemic-euglycemic clamp (insulin clamp) and saline infusion. One week before insulin clamps, indwelling carotid artery and jugular vein catheters were surgically implanted in the mice for sampling and infusions, respectively. Mice were fasted for 5 h before the start of the insulin clamp. The insulin clamps were performed as described previously (7,22,31,32). The method our laboratory uses differs from those used by most other laboratories (33,34): mice are not handled and are unstressed (32); moreover, erythrocytes are replaced to prevent a fall in hematocrit that would inevitably occur. Samples for basal arterial glucose specific activity were taken at $t = -15$ and -5 min and arterial insulin at $t = -5$ min. The clamp was initiated at $t = 0$ min with a continuous insulin infusion (4 mU $\cdot$ kg^{-1} $\cdot$ min^{-1}) that persisted for 155 min. Arterial glucose concentrations were determined at 10-min intervals to provide feedback to adjust the rate of exogenous glucose (glucose infusion rate [GIR]) as needed to clamp mice between 150 and 160 mg/dL. Steady state [3-^{3}H]glucose kinetics were determined at 10-min intervals between $t = 80$ and 120 min. Plasma insulin concentrations during the clamp were determined at $t = 100$ and 120 min. A 13 μCi injection of 2[^{14}C]deoxyglucose (2[^{14}C]2DG) was administered as an intravenous bolus at $t = 120$ min. 2[^{14}C]2DG was used to determine the glucose metabolic index (R_g), an indication of tissue-specific glucose uptake. Blood samples were collected at $t = 2$, 15, 25, and 35 min after the bolus to measure the disappearance of 2[^{14}C]DG from the plasma. Saline infusion protocols were performed using the same design as the insulin clamp, except that saline was infused and not insulin.

Glucose tolerance test (GTT). One week before mice underwent GTT, indwelling carotid artery and gastric catheters were surgically implanted for sampling and glucose administration, respectively. Mice were fasted for 5 h; then, baseline arterial glucose and insulin measurements were obtained via the arterial catheter to avoid handling of mice. Mice were then administered glucose (2 g/kg body weight) through the gastric catheter. The gastric catheter permits the mice to absorb the glucose via physiological mechanisms and avoids a stress response from intraperitoneal injection or gavage. Arterial glucose was measured at 5, 10, 15, 20, 30 45, 60, 90, and 120 min after glucose administration. Arterial insulin levels during the GTT were assessed at 10, 20, 30, 60, and 120 min.

Processing of plasma and tissue samples. Arterial insulin was determined by ELISA (ALPCO Diagnostics). Radioactivity of [3-^{3}H]glucose, 2[^{14}C]DG, and 2[^{14}C]DG-6-phosphate were assessed by liquid scintillation counting (22). R_a and R_d were calculated using non–steady-state equations (35). EndoR_a was calculated by subtraction of the GIR from total R_a. Muscle R_g was calculated as previously described (22). Liver glycogen content was determined after the insulin clamp and after a time control experiment during which saline was infused as previously reported (36). The latter experiment was useful in obtaining a measure of fasting liver glycogen for comparison with insulin clamp glycogen concentrations. Hepatic glycogen synthase activity was performed as previously described (37). Synthase activity in the presence of glucose-6-phosphate reflects the maximal enzyme activity, whereas activity in the absence of glucose-6-phosphate reflects the active form of glycogen synthase. Free fatty acids (FFA) were assessed spectrometrically by an enzymatic calorimetric assay (NEFA C Kit; Wako Chemicals). Basal FFA levels were an average of samples taken at $t = -15$ and -5 min of the insulin clamp, and the levels during the insulin clamp were the average at $t = 80$ and 120 min.

Plasma, skeletal, and cardiac VEGF levels. The gastrocnemius and cardiac muscles were homogenized as previously described (28). The plasma and tissue VEGF were assayed by the manufacturer's specifications (VEGF ELISA Kit, Mouse No. QIA52; Calbiochem), which detects $VEGF_{120}$ and $VEGF_{164}$ isoforms.

Ex vivo muscle glucose uptake. Glucose uptake was measured in isolated soleus and extensor digitorum longus muscle, as previously described (38). After a 15-min basal incubation period, muscles were transferred to fresh media and incubated for 30 min in the absence or presence of insulin (10 mU/mL). After stimulation, 2-deoxy-D-glucose uptake was measured for 10 min in fresh media, in the absence or presence of insulin, by adding cold 2-deoxy-D-glucose (1 mmol/L) and tracers 2-[1,2-^{3}H]deoxy-D-glucose (0.25μCi/mL) and D-[1-^{14}C]mannitol (0.16 Ci/mL). Muscles were then lysed, and radioactivity in the supernatant was measured using liquid scintillation counting.

Immunohistochemistry analysis of capillary density. CD31 protein was assessed by immunohistochemistry in paraffin-embedded cardiac and skeletal muscle sections (5 μm), which were incubated for 60 min with the anti-CD31 primary antibody (BD Biosciences), as previously described (7). ImageJ software was used for quantification. Muscle capillary density was determined by counting CD31-positive structures.

Immunoprecipitation and immunoblotting. Gastrocnemius and liver samples were homogenized as previously described (7). The membrane was incubated overnight at 4°C with phosphorylated Akt (Ser 473), total Akt (Cell Signaling Technology), and glyceraldehyde-3-phosphate dehydrogenase (GAPDH; Abcam) primary antibodies. For immunoprecipitation, 500 μg gastrocnemius protein supernatant was incubated with 3 μg insulin receptor substrate (IRS)-1 antibody (Santa Cruz Biotechnology) overnight at 4°C. Then, 20 μL protein A/G PLUS-Agarose (Santa Cruz Biotechnology) was added and incubated overnight at 4°C. The mixture was centrifuged at 1,000*g* and the supernatant removed. The beads were washed four times with cold PBS and centrifugation was repeated. Beads were resuspended in 30 μL NuPAGE LDS loading buffer and heated at 80°C for 5 min. Immunoblots were incubated with primary antibodies for phospho-IRS-1 (Tyr612; Invitrogen) and the p85 subunit of phosphoinositide 3-kinase (PI3K; Millipore). Secondary antibodies were incubated at room temperature for 1 h and visualization and quantification were performed using the Odyssey imaging system (LI-COR).

Real-time PCR. Total RNA was isolated from the liver using the RNeasy Mini Kit (Qiagen). Total RNA (1 mg) was reverse transcribed using the iScript cDNA Synthesis Kit (Bio-Rad). Real-time PCR was performed using TaqMan Universal PCR Master Mix (Applied Biosystems) on the CFX Real Time PCR Instrument (Bio-Rad). Data were normalized to the control gene ribosomal protein *S18*. Data were analyzed using the $2^{-\Delta\Delta Ct}$ method (39) and are presented as relative expression.

Statistical analysis. Statistical analyses were determined by Student *t* test or two-way ANOVA, followed by Tukey post hoc tests, as appropriate. Data are represented as mean ± SE. The significance level was $P \leq 0.05$.

RESULTS

Adaptations to genetic ablation of skeletal and cardiac muscle VEGF. Total body weight, fat, or lean masses did not differ in mice at age 12 weeks (Table 1). VEGF levels in cardiac and skeletal muscle of *mVEGF*$^{-/-}$ mice were undetectable, compared with ~30 pg/mg protein in cardiac and skeletal muscle of *mVEGF*$^{+/+}$ littermates ($P \leq 0.001$; Fig. 1*A*). The reduction in VEGF protein corresponded to 60% and 50% decreases in capillary density in skeletal and cardiac muscle, respectively ($P \leq 0.05$; Table 1). Plasma VEGF levels were similar in both groups (Fig. 1*B*). Cardiac output was equal between genotypes (Table 1), because heart rate and stroke volume, calculated from the echocardiography, did not differ (data not shown). Furthermore, mean arterial pressure was similar between genotypes (Table 1). Left ventricular (LV) volume and LV mass were significantly increased in the *mVEGF*$^{-/-}$

TABLE 1
Characteristics of muscle-specific VEGF-deficient mice

	mVEGF$^{+/+}$ $n = 8$	*mVEGF*$^{-/-}$ $n = 9$
Weight (g)	26.1 ± 1.5	25.3 ± 0.9
Fat (g)	2.2 ± 0.3	2.1 ± 0.2
Muscle (g)	18.5 ± 1.2	18.0 ± 0.7
Capillary density†		
Gastrocnemius	1.00 ± 0.20	0.41 ± 0.10*
Cardiac	1.00 ± 0.06	0.52 ± 0.06*
Mean arterial pressure (mmHg)	117 ± 4.0	108 ± 4.4
Cardiac output (mL/min)	23.9 ± 1.7	21.0 ± 0.6
Fractional shortening (%)	46.6 ± 1.2	18.7 ± 2.0*
Ejection fraction (%)	78.9 ± 1.3	38.5 ± 3.7*
LV diastolic volume (μL)	47.3 ± 4.0	89.5 ± 7.0*
LV mass (mg)	54.6 ± 5.5	66.9 ± 3.4*

Data are expressed as mean ± SE. †Gastrocnemius and cardiac capillary density were quantified by the number of CD31$^+$ structures normalized to *mVEGF*$^{+/+}$ mice. *$P \leq 0.05$.

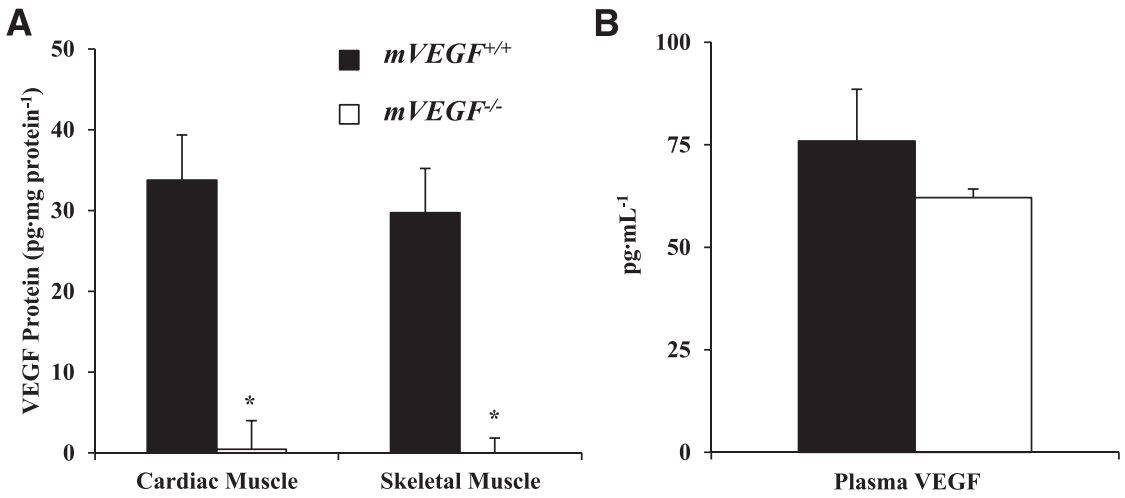

FIG. 1. VEGF-A protein levels in tissue homogenates from cardiac and skeletal muscle (*A*) and VEGF-A plasma concentration (*B*). Skeletal muscle VEGF levels were quantified in the gastrocnemius. Values are expressed as means ± SE (n = 5). *$P \leq 0.05$ vs. $mVEGF^{+/+}$.

mice but ejection fraction and fractional shortening were 2- and 2.5-fold lower ($P \leq 0.05$; Table 1).

***mVEGF*$^{-/-}$ mice have impaired insulin-stimulated glucose disposal and augmented fasting hepatic glucose turnover.** Basal (5-h fasting) and insulin clamp arterial glucose and insulin did not differ between genotypes (Table 2). The basal circulating FFA concentrations and the suppression of FFA by insulin were similar between genotypes (Table 2). The steady-state GIRs were equal (Fig. 2*B*). Fasting endogenous glucose production ($EndoR_a$) and glucose disappearance (R_d) were 1.6-fold greater in $mVEGF^{-/-}$ mice ($P \leq 0.05$; Fig. 2*C* and *D*). The relative gene expression for phosphoenolpyruvate carboxykinase (*PEPCK*; Fig. 3*D*) was not different between genotypes; however, glucose-6-phosphatase (*G6Pase*; Fig. 3*D*; $P \leq 0.05$) was higher in $mVEGF^{-/-}$ mice and might contribute to the augmented fasting $EndoR_a$. The suppression of $EndoR_a$ and the absolute whole-body R_d during insulin stimulation were similar between groups (Fig. 2*C* and *D*). Notably, the increase in insulin-stimulated glucose disposal was blunted by 56 ± 16% in the $mVEGF^{-/-}$ mice, suggesting an impairment in peripheral insulin action ($P \leq 0.05$; Fig. 2*E*). The results from the GTTs (Fig. 3*A*) indicated that $mVEGF^{-/-}$ mice were less glucose-tolerant than their wild-type littermates. The area under the curve for the first 30 min ($P \leq 0.05$; Fig. 3*C*) of the GTT was greater in the $mVEGF^{-/-}$ mice, and the insulin response did not differ except at 60 min (Fig. 3*B*).

TABLE 2
Fasting and insulin clamp characteristics

	$mVEGF^{+/+}$	$mVEGF^{-/-}$
Arterial glucose (mg/dL)		
Basal	119 ± 7	113 ± 5
Insulin clamp	145 ± 3	151 ± 3
Arterial insulin (ng/mL)		
Basal	1.2 ± 0.2	1.6 ± 0.3
Insulin clamp	4.2 ± 0.8	5.2 ± 0.5
FFA (mmol/L)		
Basal	0.76 ± 0.10	0.76 ± 0.10
Insulin clamp	0.18 ± 0.04	0.17 ± 0.01
Liver glycogen†	10.0 ± 2.3	18.6 ± 2.1*
Fasting liver glycogen†	3.90 ± 2.0	8.30 ± 1.9
Glycogen synthase activity‡	0.06 ± 0.007	0.09 ± 0.015

Data are expressed as mean ± SE (n = 7–9). †Liver glycogen (mg glucose/g liver) was measured from tissue excised immediately after the insulin clamp, and fasting liver glycogen (mg glucose/g liver) was assessed immediately after the 7.5-h saline-infused experiments. ‡Liver glycogen synthase activity was determined after the insulin clamp and is presented as the ratio of glycogen synthase activity in the absence and presence of glucose-6-phosphate. *$P \leq 0.05$.

Consistent with the impairment in insulin-stimulated whole-body R_d, insulin-stimulated R_g in skeletal and cardiac muscle in $mVEGF^{-/-}$ mice was also abated compared with $mVEGF^{+/+}$ littermates ($P \leq 0.05$; Fig. 4*A* and *B*). Insulin-stimulated R_g is the difference between the R_g during the insulin clamp and an average R_g from the saline-infused mice. The data obtained from these saline-infused time controls permit the quantification of the specific effect of insulin on R_g. Furthermore, in vivo insulin signaling in skeletal muscle was attenuated during the insulin clamp, evident by a decrease in the association of the p85 subunit of PI3K with phospho-IRS-1 ($P \leq 0.05$; Fig. 5*B*). Interestingly, downstream Akt activation, which is central to multiple signaling pathways in muscle, was unaffected during the insulin clamp (Fig. 5*D*).

Muscle insulin action is decreased in *mVEGF*$^{-/-}$ mice in vivo but not in vitro. Glucose uptake was analyzed in isolated muscle, thus removing the extramyocellular barriers to MGU. Isolated MGU was determined on the soleus (slow-twitch) and extensor digitorum longus (fast-twitch) muscles. Basal and insulin-stimulated glucose uptake in isolated skeletal muscles were equal between genotypes (Fig. 6), suggesting no direct impairment of insulin action at the myocyte. The data in isolated muscle contrasts with the muscle glucose uptake and insulin-signaling data from the insulin clamp, which were diminished as described above. These data indicate insulin action was impaired by muscle VEGF deletion in the whole organism where extramyocellular factors are present but not in isolated muscle where they are not. This strongly suggests that muscle VEGF deletion results in resistance to insulin because of an impaired capacity to deliver insulin to the sarcolemma.

Liver glycogen content was greater in *mVEGF*$^{-/-}$ mice after the insulin clamp. Whole-body R_d was elevated in the basal state of $mVEGF^{-/-}$ mice and equal during the insulin clamp. Liver glycogen content was

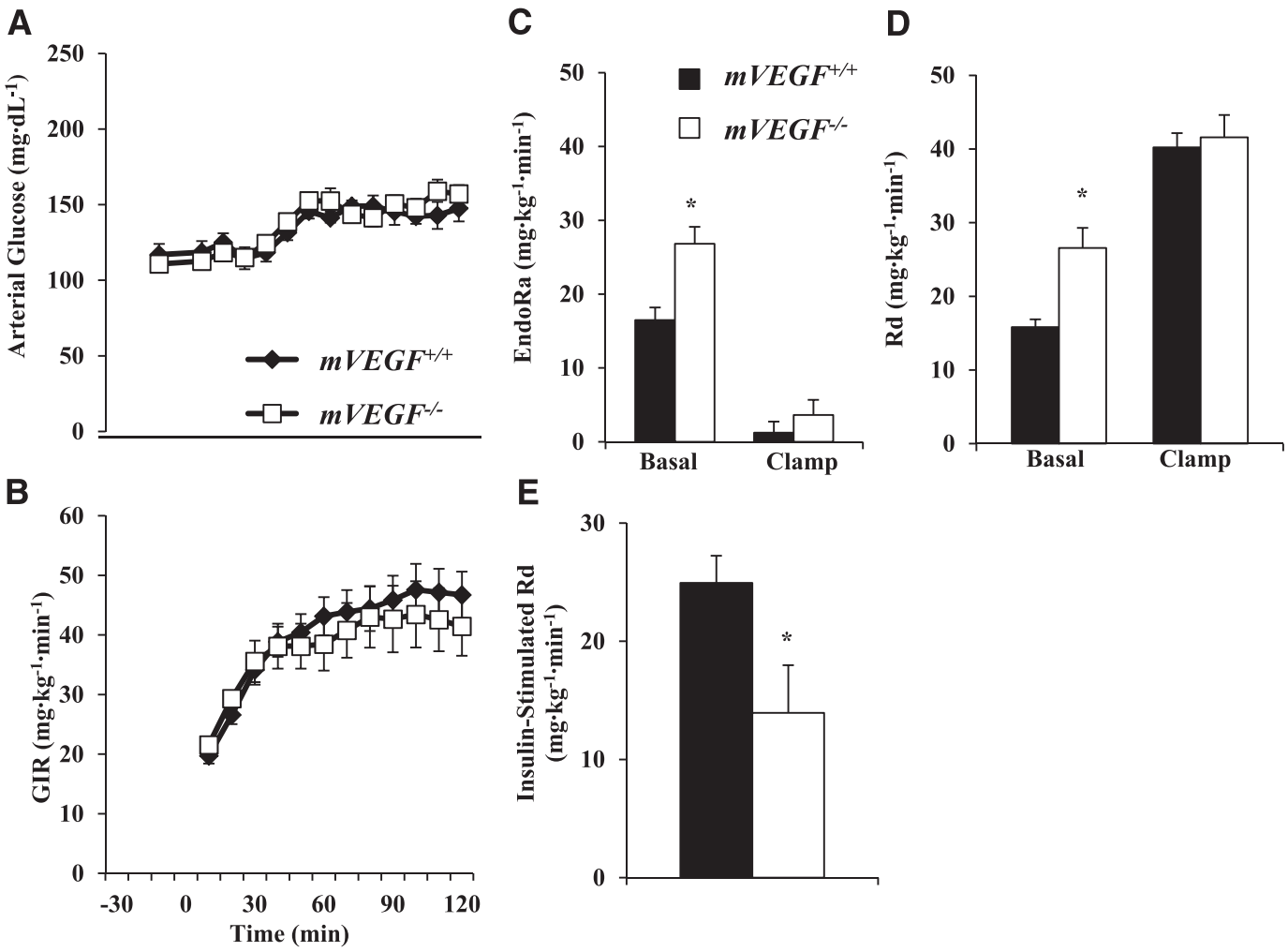

FIG. 2. Arterial glucose (*A*) and glucose infusion rate (*B*) during the hyperinsulinemic-euglycemic clamp. Mice were fasted 5 h before the onset of the clamp. Blood glucose was maintained at ~150 mg/dL during steady-state (80–120 min), and the time course is displayed to demonstrate quality of the clamp. Glucose (50%) was infused to maintain euglycemia. EndoR_a (*C*), whole-body R_d, (*D*), and insulin-stimulated glucose disposal (*E*) were determined during the hyperinsulinemic-euglycemic clamp. Basal values were determined from samples at −15 and −5 min before the onset of the clamp, and insulin clamp levels were calculated from steady-state values (80–120 min). Insulin-stimulated R_d was calculated by subtracting the basal R_d from the clamp R_d, which measures the increase in insulin-stimulated glucose disposal. Data are expressed as mean ± SE (n = 7–9). *$P \leq 0.05$ vs. *mVEGF*$^{+/+}$.

assessed after the insulin clamp to test the possibility that liver glucose uptake was compensating for the impaired insulin-stimulated MGU. Consistent with this possibility, *mVEGF*$^{-/-}$ mice had an approximately twofold increase in liver glycogen concentrations compared with *mVEGF*$^{+/+}$ littermates ($P \leq 0.05$; Table 2). During the time control experiment, where saline was infused in lieu of insulin, fasting (7.5-h) liver glycogen levels (Table 2) were minimal, and there was no significant difference between genotypes. The greater hepatic glycogen concentration in the *mVEGF*$^{-/-}$ mice was independent of changes in phosphorylation of Akt in the liver (Fig. 5*F*) during the insulin clamp. Hepatic glycogen synthase activity was assessed after the insulin clamp. *mVEGF*$^{-/-}$ mice tended to have greater glycogen synthase activity (P = 0.08; Table 2), which likely contributes to the greater liver glycogen content after the insulin clamp. Thus, indirect adaptations at the liver may counterbalance the diminished insulin-stimulated MGU and explain the similar total glucose utilization between the two genotypes during insulin stimulation (Fig. 2*B*).

DISCUSSION

These studies demonstrate that capillary rarefaction impairs muscle insulin action in vivo. Our data support the paradigm that capillary regression contributes to the pathogenesis of skeletal muscle insulin resistance. Diabetic states are characterized by muscle capillary regression that results from impaired VEGF action (21,29). Here we show that local VEGF deletion is sufficient to cause muscle insulin resistance due to diminished muscle capillary density. Although the decrease in muscle capillaries is substantive, it is also possible that an alteration occurs in the vessel wall that affects permeability to insulin. Previous studies have shown muscle capillarity strongly correlates with insulin sensitivity (19,20). Furthermore, therapeutic treatments that reverse muscle insulin resistance in mice augment capillary density (7,9). Our data illustrate that attenuating capillarity specifically in muscle blunts insulin-stimulated R_d due to diminished muscle R_g (Fig. 2*E* and Fig. 4), without directly affecting myocellular insulin action (Fig. 6). In addition, *mVEGF*$^{-/-}$ mice were less glucose-tolerant than

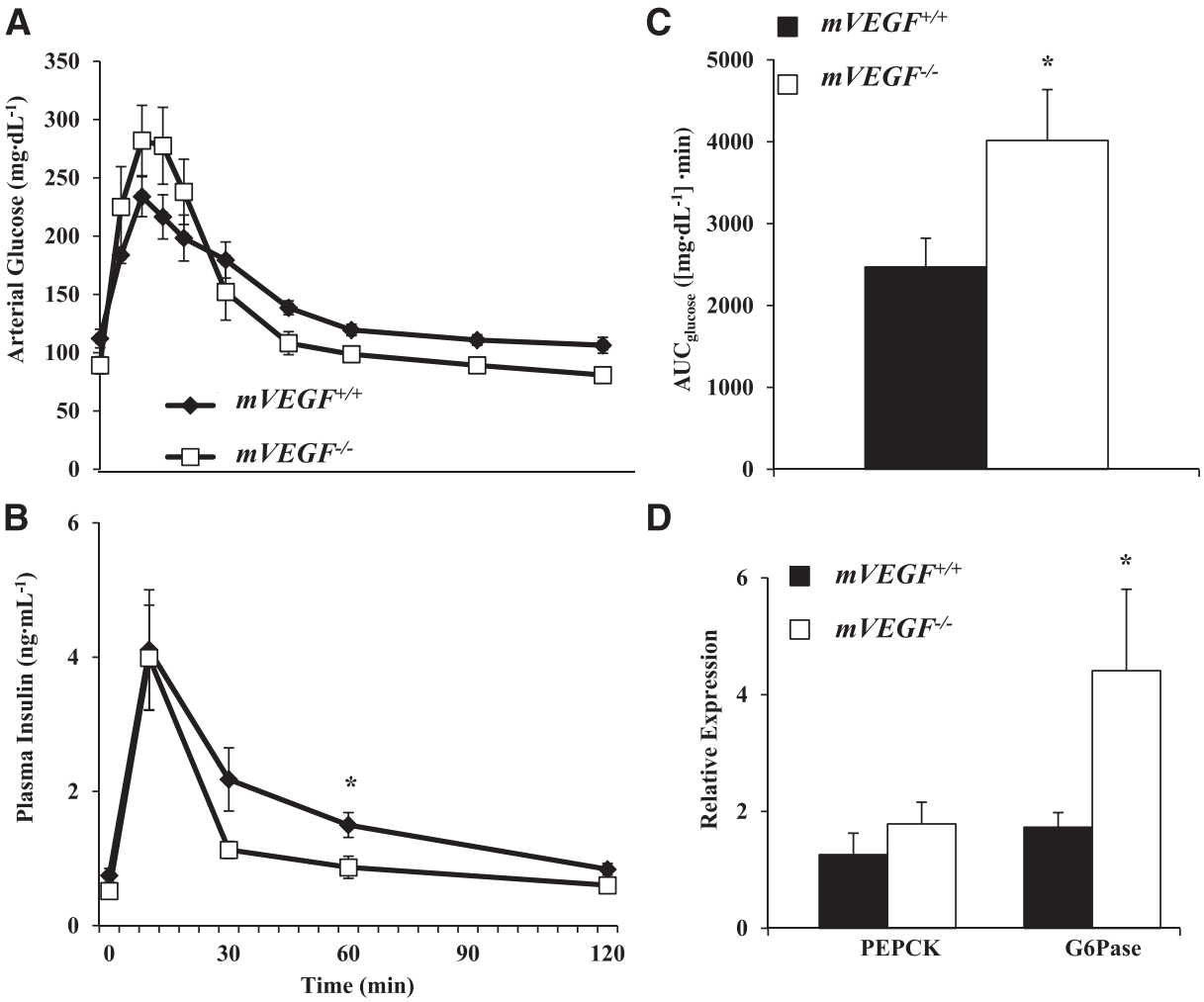

FIG. 3. Glucose tolerance was determined (*A*), and corresponding plasma insulin levels were quantified (*B*) on 5-h fasted mice. *C*: The area under the curve was determined from 0 to 30 min and normalized to fasting arterial glucose concentration. *D*: RT-PCR was performed on hepatic RNA extracts from mice fasted for 5 h for the relative expression of the gluconeogenic genes *PEPCK* and *G6Pase*. Values are expressed as mean ± SE (n = 5–6). *$P \leq 0.05$ vs. *mVEGF*$^{+/+}$.

their wild-type littermates (Fig. 3*C*), despite similar insulin responses to a glucose load (Fig. 3*B*). These data emphasize the importance of increased muscle blood volume and capillary surface area for the delivery of insulin and glucose to skeletal muscle during hyperinsulinemia (2,12,14).

The reduced insulin-stimulated MGU in *mVEGF*$^{-/-}$ mice was not attributable to impaired insulin action directly at

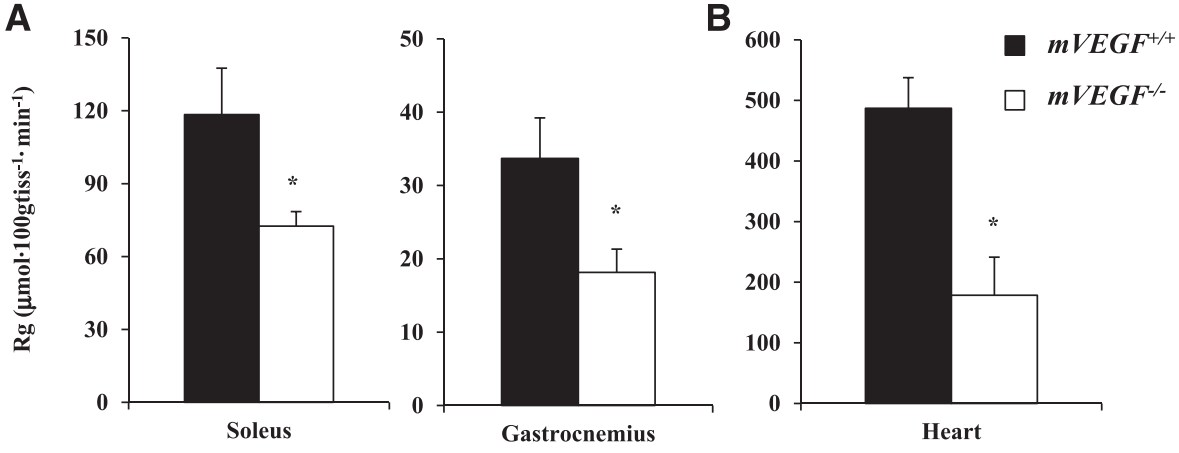

FIG. 4. Insulin-stimulated R_g in skeletal (*A*) and cardiac (*B*) muscle. To quantify insulin-stimulated R_g, we performed a time control in a cohort of *mVEGF*$^{+/+}$ and *mVEGF*$^{-/-}$ mice in which saline was infused in lieu of insulin to quantify basal R_g. The R_g values from the saline infusion were averaged and subtracted from the R_g values during the insulin clamp. Data are expressed as mean ± SE (n = 7–9). *$P \leq 0.05$ vs. *mVEGF*$^{+/+}$.

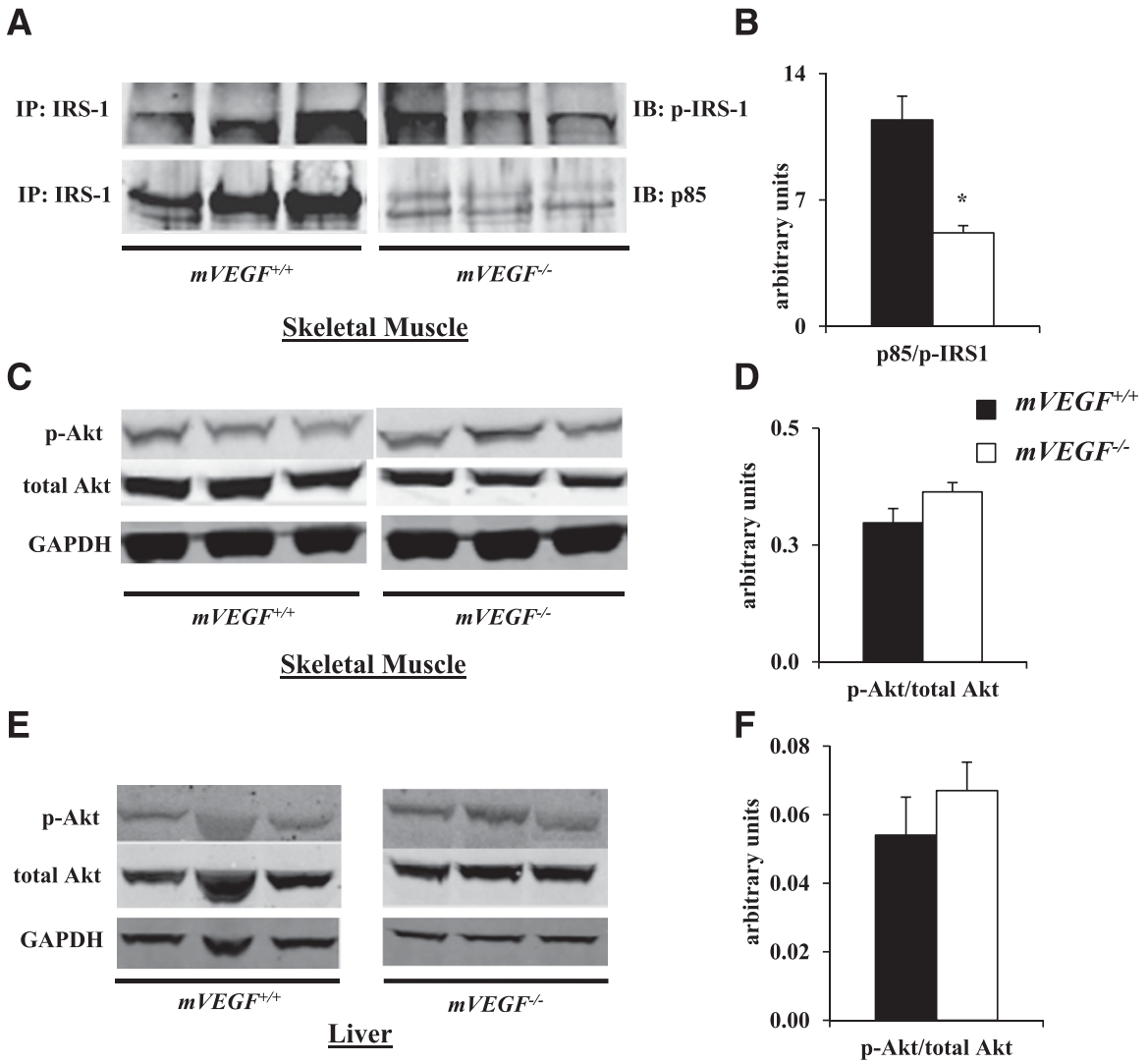

FIG. 5. Skeletal muscle and hepatic insulin signaling after the hyperinsulinemic-euglycemic clamp. Western blot analysis was performed on extracts of the gastrocnemius and liver for the phosphorylation (p) of Akt at Ser473 and total Akt. Infrared imaging was performed on 4–12% SDS-PAGE gel in skeletal muscle (*A* and *C*) and liver (*E*). *A*: Immunoprecipitation (IP) from gastrocnemius extracts were performed with total IRS-1; then, immunoblots (IB) were completed for p-IRS-1 at Tyr612 and the p85 subunit of PI3K. *B*: Insulin-stimulated p85 association with p-IRS-1 was quantified as the ratio of p85–to–p-IRS-1. Insulin activation of Akt (*C* and *E*) was quantified as the ratio of p-Akt to total Akt in skeletal muscle (*D*) and liver (*F*). GAPDH was used as a loading control. Data are expressed as mean ± SE (n = 5–6). *$P \leq 0.05$ vs. $mVEGF^{+/+}$.

the myocyte; however, in vivo insulin signaling during hyperinsulinemia was blunted in $mVEGF^{-/-}$ mice, suggesting a defect in insulin delivery. There was no difference in ex vivo insulin-mediated glucose uptake in isolated muscles (Fig. 6). Measuring glucose uptake in isolated muscle removes the vascular delivery component of MGU, eliminating the difference between genotypes evident during the insulin clamp. Skeletal muscle does not express VEGF receptors, indicating the decrease in muscle VEGF does not have direct effects at the myocyte (40). The association of the p85 subunit of PI3K with phospho-IRS-1 during the insulin clamp was attenuated in $mVEGF^{-/-}$ mice, although skeletal muscle Akt activation was preserved (Fig. 5*B* and *D*). Kim et al. (41) demonstrated that insulin-stimulated phosphorylation of Akt in diabetic muscle was normal and that the primary deficiency in insulin signaling was attributed to a decrease in PI3K association with IRS-1. Our data are consistent with studies that showed the critical role of glucose and insulin delivery to insulin-stimulated MGU (3,4,13,22,42). Moreover, in genetic- and diet-induced models of muscle insulin resistance, the physiological actions of insulin to increase muscle microvascular recruitment and nutrient blood flow are impaired, resulting in an abatement in insulin and glucose delivery to the myocyte (4,6,16,43,44). The present data demonstrate that the attenuation in muscle capillary density associated with insulin resistance, in the absence of other primary defects, is capable of seriously diminishing insulin-stimulated MGU due to decreases in insulin and, likely, glucose delivery to the myocyte. It is also possible that other nutritional or endocrine factors that are deficient with poor muscle perfusion are necessary for the full response to insulin in vivo. These studies clearly demonstrate that a loss in muscle capillaries causes a marked impairment in muscle insulin action, thus supporting the paradigm that capillary rarefaction in insulin-resistant human skeletal muscle is not simply a consequence of the disease but central to the pathogenesis of muscle insulin resistance.

At rest, ~30% of capillaries are required to maintain the demand for skeletal muscle perfusion (45,46). As a result

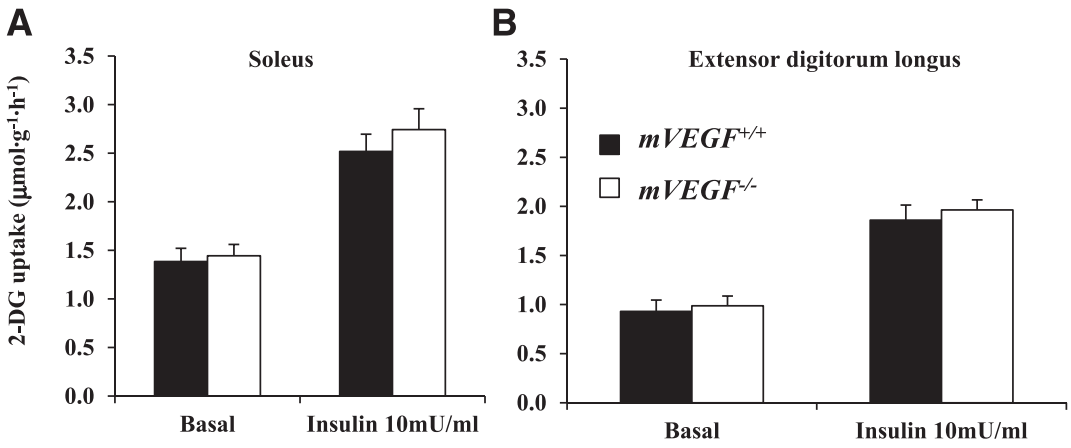

FIG. 6. Skeletal muscle insulin action was assessed in the isolated soleus (*A*) and extensor digitorum longus (*B*). Mice were fasted for 5 h before the excision of the muscles. Values are expressed as mean ± SE (n = 6).

of the low number of capillaries necessary to maintain nutrient blood flow, there was no defect in fasting MGU in $mVEGF^{-/-}$ mice (data not shown). Physiological hyperinsulinemia recruits unperfused capillaries, doubling the microvascular blood volume in the muscle (43,47). The augmented insulin and glucose delivery to the muscle interstitium during hyperinsulinemia is dependent on the increased surface area for substrate exchange induced by insulin-mediated capillary recruitment (42,43,47). The ~60% attenuation in skeletal muscle capillary density in $mVEGF^{-/-}$ mice resulted in an impairment in glucose uptake during steady-state hyperinsulinemia. This effect is similar to the decrease in capillary recruitment that prevents an increase in muscle blood volume and impairs muscle insulin action in obese, type 2 diabetic individuals (43).

In our model of muscle-specific VEGF deletion, Cre recombinase is under the *MCK* promoter, which is not expressed until fetal day 16 and then is upregulated after birth (48). This time course of *VEGF* ablation limits developmental abnormalities. *VEGF* expression is critical for embryonic development and the loss of a single *VEGF* allele in the whole organism causes embryonic death, with developmental abnormalities evident by day 9.5 of gestation (49,50). Furthermore, endothelial-specific deletion of VEGF results in endothelial apoptosis and sudden death in 55% of mutant mice by age 25 weeks, which indicates the importance of autocrine VEGF signaling in the maintenance of endothelial integrity in the adult animal (51). Olfert et al. (28) showed in muscle-specific VEGF-deficient mice that the attenuation in skeletal muscle capillary density occurs as early as age 1 month. The myocellular paracrine signaling of VEGF is essential for the spatial branching of the capillary network and is necessary for muscle capillary architectural organization (29,52,53). The capillaries present in $mVEGF^{-/-}$ mice are likely a combination of refractory capillaries, VEGF independent capillaries, and vessels present before *MCK* expression that are maintained by autocrine endothelial VEGF signaling.

Diabetic states are characterized by cardiac muscle capillary regression and impaired VEGF action (25,26). Severe hyperglycemia downregulates VEGF expression, which is seminal in the pathology of diabetic cardiomyopathy (54). Endothelial cells are particularly sensitive to changes in plasma glucose because they are very permeable to glucose. VEGF ablation in our model resulted in a 50% decrease in cardiac capillary density. Notably, compensatory mechanisms kept cardiac output normal (Table 1). The conserved cardiac output is a mathematical consequence of the decreased ejection fraction coupled with the increase in LV diastolic volume. The potential relationship of this to the underlying vascular pathology must be speculative at this point. The thinner but larger ventricular cavity might entail less mural resistance to flow, allowing better capillary perfusion pressure through an attenuated vascular network. Alternatively, the larger endocardial surface area might allow some direct supply of oxygen and nutrients to the immediately adjacent myocardium, a mechanism important in the right ventricle but potentially significant for the LV in $mVEGF^{-/-}$ mice. Although the dilation in our model is common to many cardiomyopathic conditions, the preservation of cardiac output may be a consequence of this specific etiology.

Basal glucose flux was elevated in $mVEGF^{-/-}$ mice compared with $mVEGF^{+/+}$ littermates (Fig. 2). Glucose homeostasis was maintained, despite the elevated glucose fluxes. $mVEGF^{-/-}$ mice had greater liver glycogen deposition after the insulin clamp; however, fasting hepatic glycogen did not differ significantly between the two genotypes (Table 2). The greater liver glycogen deposition in $mVEGF^{-/-}$ mice may offset the reduction in insulin-stimulated muscle R_g, explaining the equal GIRs and absolute whole-body R_d during the insulin clamp. The augmented liver glycogen after the insulin clamp was independent of the phosphorylation status of Akt in the liver (Fig. 5*F*). However, glycogen synthase activity tended to be augmented in $mVEGF^{-/-}$ mice (Table 2). The elevated activity of glycogen synthase likely contributes to the higher hepatic glycogen concentrations in $mVEGF^{-/-}$ mice after the insulin clamp. The presence of G6Pase in the liver obviates the use of isotopic 2-deoxyglucose to measure R_g in the liver; thus, no precise measurement of hepatic glucose uptake can be determined with the insulin clamp protocol performed in the current studies. Moreover, the increased basal glucose turnover suggests accelerated hepatic cycling of glucose independent of hepatic insulin action (55). The increased fasting EndoR_a may be due to the greater *G6Pase* expression in the liver of $mVEGF^{-/-}$ mice (Fig. 3*D*). The mechanism behind the hepatic adaptation is unclear; however, it is notable that untreated insulin-resistant humans also have accelerated glucose production.

The compensatory mechanisms in the *mVEGF*$^{-/-}$ mice cannot be attributed to changes in circulating VEGF levels (Fig. 1*B*). Thus, the deletion of all VEGF-A variants in muscle is not likely to have direct physiological effects on other tissues. The compensation present in the liver is expected to be a consequence of the impaired insulin-stimulated MGU or perhaps inflammation secondary to heart or skeletal muscle hypoxia resulting from poor perfusion.

These data show for the first time that a reduction in capillary density is sufficient to induce muscle insulin resistance in lean mice. The present investigation is consistent with human data that exhibit a strong relationship between muscle capillary density and insulin-mediated peripheral glucose disposal (18,20,56). The results further elucidate the significance of the extramyocellular adaptations present in insulin-resistant states, thus, highlighting the importance for novel therapeutic approaches to target the vascular bed of insulin-sensitive tissues in the treatment of insulin resistance and type 2 diabetes.

ACKNOWLEDGMENTS

This work was supported by National Institutes of Health Grants DK-054902 and DK-059637 to the VMMPC.

No potential conflicts of interest relevant to this article were reported.

J.S.B. researched data and wrote the manuscript. L.L. and C.M.H. researched data and reviewed the manuscript. F.D.J. and D.P.B. researched data. D.H.W. contributed to discussion and reviewed the manuscript. D.H.W. is the guarantor of this work, and, as such, had full access to data and takes full responsibility for the integrity of data and accuracy of data analysis.

Parts of this study were presented in abstract form at the 72nd Scientific Sessions of the American Diabetes Association, Philadelphia, Pennsylvania, 8–12 June 2012.

The authors thank ZhiZhang Wang of the VMMPC Cardiovascular Pathophysiology Core for performing echocardiography in these studies, Melissa B. Downing of the Mouse Pathology Core Laboratory of the VMMPC, and Dr. Jeffrey N. Rottman for his insightful comments interpreting the echocardiography results.

REFERENCES

1. DeFronzo RA, Ferrannini E. Insulin resistance. A multifaceted syndrome responsible for NIDDM, obesity, hypertension, dyslipidemia, and atherosclerotic cardiovascular disease. Diabetes Care 1991;14:173–194
2. Vincent MA, Barrett EJ, Lindner JR, Clark MG, Rattigan S. Inhibiting NOS blocks microvascular recruitment and blunts muscle glucose uptake in response to insulin. Am J Physiol Endocrinol Metab 2003;285:E123–E129
3. Fueger PT, Shearer J, Bracy DP, et al. Control of muscle glucose uptake: test of the rate-limiting step paradigm in conscious, unrestrained mice. J Physiol 2005;562:925–935
4. Halseth AE, Bracy DP, Wasserman DH. Limitations to basal and insulin-stimulated skeletal muscle glucose uptake in the high-fat-fed rat. Am J Physiol Endocrinol Metab 2000;279:E1064–E1071
5. Chiu JD, Richey JM, Harrison LN, et al. Direct administration of insulin into skeletal muscle reveals that the transport of insulin across the capillary endothelium limits the time course of insulin to activate glucose disposal. Diabetes 2008;57:828–835
6. Ellmerer M, Hamilton-Wessler M, Kim SP, et al. Reduced access to insulin-sensitive tissues in dogs with obesity secondary to increased fat intake. Diabetes 2006;55:1769–1775
7. Kang L, Ayala JE, Lee-Young RS, et al. Diet-induced muscle insulin resistance is associated with extracellular matrix remodeling and interaction with integrin alpha2beta1 in mice. Diabetes 2011;60:416–426
8. Frisbee JC. Hypertension-independent microvascular rarefaction in the obese Zucker rat model of the metabolic syndrome. Microcirculation 2005;12:383–392
9. Guo Q, Mori T, Jiang Y, et al. Losartan modulates muscular capillary density and reverses thiazide diuretic-exacerbated insulin resistance in fructose-fed rats. Hypertens Res 2012;35:48–54
10. Berria R, Wang L, Richardson DK, et al. Increased collagen content in insulin-resistant skeletal muscle. Am J Physiol Endocrinol Metab 2006;290:E560–E565
11. Solomon TP, Haus JM, Li Y, Kirwan JP. Progressive hyperglycemia across the glucose tolerance continuum in older obese adults is related to skeletal muscle capillarization and nitric oxide bioavailability. J Clin Endocrinol Metab 2011;96:1377–1384
12. Vincent MA, Clerk LH, Lindner JR, et al. Microvascular recruitment is an early insulin effect that regulates skeletal muscle glucose uptake in vivo. Diabetes 2004;53:1418–1423
13. Baron AD, Laakso M, Brechtel G, Edelman SV. Mechanism of insulin resistance in insulin-dependent diabetes mellitus: a major role for reduced skeletal muscle blood flow. J Clin Endocrinol Metab 1991;73:637–643
14. Baron AD, Tarshoby M, Hook G, et al. Interaction between insulin sensitivity and muscle perfusion on glucose uptake in human skeletal muscle: evidence for capillary recruitment. Diabetes 2000;49:768–774
15. Kim F, Pham M, Maloney E, Rizzo NO, Morton GJ, Wisse BE, Kirk EA, Chait A, Schwartz MW. Vascular inflammation, insulin resistance, and reduced nitric oxide production precedes the onset of peripheral insulin resistance. Arterioscler Thromb Vasc Biol 2008;28:1982–1988
16. Kubota T, Kubota N, Kumagai H, et al. Impaired insulin signaling in endothelial cells reduces insulin-induced glucose uptake by skeletal muscle. Cell Metab 2011;13:294–307
17. Laakso M, Edelman SV, Brechtel G, Baron AD. Decreased effect of insulin to stimulate skeletal muscle blood flow in obese man. A novel mechanism for insulin resistance. J Clin Invest 1990;85:1844–1852
18. Gavin TP, Stallings HW 3rd, Zwetsloot KA, et al. Lower capillary density but no difference in VEGF expression in obese vs. lean young skeletal muscle in humans. J Appl Physiol 2005;98:315–321
19. Lillioja S, Young AA, Culter CL, et al. Skeletal muscle capillary density and fiber type are possible determinants of in vivo insulin resistance in man. J Clin Invest 1987;80:415–424
20. Mårin P, Andersson B, Krotkiewski M, Björntorp P. Muscle fiber composition and capillary density in women and men with NIDDM. Diabetes Care 1994;17:382–386
21. Chung AW, Hsiang YN, Matzke LA, McManus BM, van Breemen C, Okon EB. Reduced expression of vascular endothelial growth factor paralleled with the increased angiostatin expression resulting from the upregulated activities of matrix metalloproteinase-2 and -9 in human type 2 diabetic arterial vasculature. Circ Res 2006;99:140–148
22. Ayala JE, Bracy DP, Julien BM, Rottman JN, Fueger PT, Wasserman DH. Chronic treatment with sildenafil improves energy balance and insulin action in high fat-fed conscious mice. Diabetes 2007;56:1025–1033
23. Chai W, Wang W, Dong Z, Cao W, Liu Z. Angiotensin II receptors modulate muscle microvascular and metabolic responses to insulin in vivo. Diabetes 2011;60:2939–2946
24. Olsson AK, Dimberg A, Kreuger J, Claesson-Welsh L. VEGF receptor signalling - in control of vascular function. Nat Rev Mol Cell Biol 2006;7:359–371
25. Chou E, Suzuma I, Way KJ, et al. Decreased cardiac expression of vascular endothelial growth factor and its receptors in insulin-resistant and diabetic States: a possible explanation for impaired collateral formation in cardiac tissue. Circulation 2002;105:373–379
26. Sasso FC, Torella D, Carbonara O, et al. Increased vascular endothelial growth factor expression but impaired vascular endothelial growth factor receptor signaling in the myocardium of type 2 diabetic patients with chronic coronary heart disease. J Am Coll Cardiol 2005;46:827–834
27. Hazarika S, Dokun AO, Li Y, Popel AS, Kontos CD, Annex BH. Impaired angiogenesis after hindlimb ischemia in type 2 diabetes mellitus: differential regulation of vascular endothelial growth factor receptor 1 and soluble vascular endothelial growth factor receptor 1. Circ Res 2007;101:948–956
28. Olfert IM, Howlett RA, Tang K, et al. Muscle-specific VEGF deficiency greatly reduces exercise endurance in mice. J Physiol 2009;587:1755–1767
29. Tang K, Breen EC, Gerber HP, Ferrara NMA, Wagner PD. Capillary regression in vascular endothelial growth factor-deficient skeletal muscle. Physiol Genomics 2004;18:63–69
30. Gerber HP, Hillan KJ, Ryan AM, et al. VEGF is required for growth and survival in neonatal mice. Development 1999;126:1149–1159
31. Berglund ED, Li CY, Poffenberger G, et al. Glucose metabolism in vivo in four commonly used inbred mouse strains. Diabetes 2008;57:1790–1799
32. Ayala JE, Bracy DP, McGuinness OP, Wasserman DH. Considerations in the design of hyperinsulinemic-euglycemic clamps in the conscious mouse. Diabetes 2006;55:390–397

33. Jornayvaz FR, Birkenfeld AL, Jurczak MJ, et al. Hepatic insulin resistance in mice with hepatic overexpression of diacylglycerol acyltransferase 2. Proc Natl Acad Sci U S A 2011;108:5748–5752
34. Kim HJ, Higashimori T, Park SY, et al. Differential effects of interleukin-6 and -10 on skeletal muscle and liver insulin action in vivo. Diabetes 2004; 53:1060–1067
35. Steele R, Wall JS, De Bodo RC, Altszuler N. Measurement of size and turnover rate of body glucose pool by the isotope dilution method. Am J Physiol 1956;187:15–24
36. Chan TM, Exton JH. A rapid method for the determination of glycogen content and radioactivity in small quantities of tissue or isolated hepatocytes. Anal Biochem 1976;71:96–105
37. Golden S, Wals PA, Katz J. An improved procedure for the assay of glycogen synthase and phosphorylase in rat liver homogenates. Anal Biochem 1977;77:436–445
38. Jørgensen SB, Viollet B, Andreelli F, et al. Knockout of the alpha2 but not alpha1 5'-AMP-activated protein kinase isoform abolishes 5-amino-imidazole-4-carboxamide-1-beta-4-ribofuranosidebut not contraction-induced glucose uptake in skeletal muscle.. J Biol Chem 2004;279:1070–1079
39. Pfaffl MW. A new mathematical model for relative quantification in real-time RT-PCR. Nucleic Acids Res 2001;29:e45
40. Arsic N, Zacchigna S, Zentilin L, et al. Vascular endothelial growth factor stimulates skeletal muscle regeneration in vivo. Mol Ther 2004;10:844–854
41. Kim YB, Nikoulina SE, Ciaraldi TP, Henry RR, Kahn BB. Normal insulin-dependent activation of Akt/protein kinase B, with diminished activation of phosphoinositide 3-kinase, in muscle in type 2 diabetes. J Clin Invest 1999;104:733–741
42. Barrett EJ, Wang H, Upchurch CT, Liu Z. Insulin regulates its own delivery to skeletal muscle by feed-forward actions on the vasculature. Am J Physiol Endocrinol Metab 2011;301:E252–E263
43. Clerk LH, Vincent MA, Jahn LA, Liu Z, Lindner JR, Barrett EJ. Obesity blunts insulin-mediated microvascular recruitment in human forearm muscle. Diabetes 2006;55:1436–1442
44. Sjöstrand M, Gudbjörnsdottir S, Holmäng A, Lönn L, Strindberg L, Lönnroth P. Delayed transcapillary transport of insulin to muscle interstitial fluid in obese subjects. Diabetes 2002;51:2742–2748
45. Lindbom L. Microvascular blood flow distribution in skeletal muscle. An intravital microscopic study in the rabbit. Acta Physiol Scand Suppl 1983; 525:1–40
46. Honig CR, Odoroff CL, Frierson JL. Active and passive capillary control in red muscle at rest and in exercise. Am J Physiol 1982;243:H196–H206
47. de Jongh RT, Clark AD, IJzerman RG, Serné EH, de Vries G, Stehouwer CD. Physiological hyperinsulinaemia increases intramuscular microvascular reactive hyperaemia and vasomotion in healthy volunteers. Diabetologia 2004;47:978–986.
48. Trask RV, Billadello JJ. Tissue-specific distribution and developmental regulation of M and B creatine kinase mRNAs. Biochim Biophys Acta 1990; 1049:182–188
49. Carmeliet P, Ferreira V, Breier G, et al. Abnormal blood vessel development and lethality in embryos lacking a single VEGF allele. Nature 1996;380:435–439
50. Ferrara N, Carver-Moore K, Chen H, et al. Heterozygous embryonic lethality induced by targeted inactivation of the VEGF gene. Nature 1996; 380:439–442
51. Lee S, Chen TT, Barber CL, et al. Autocrine VEGF signaling is required for vascular homeostasis. Cell 2007;130:691–703
52. Ruhrberg C, Gerhardt H, Golding M, et al. Spatially restricted patterning cues provided by heparin-binding VEGF-A control blood vessel branching morphogenesis. Genes Dev 2002;16:2684–2698
53. Giordano FJ, Gerber HP, Williams SP, et al. A cardiac myocyte vascular endothelial growth factor paracrine pathway is required to maintain cardiac function. Proc Natl Acad Sci U S A 2001;98:5780–5785
54. Yoon YS, Uchida S, Masuo O, et al. Progressive attenuation of myocardial vascular endothelial growth factor expression is a seminal event in diabetic cardiomyopathy: restoration of microvascular homeostasis and recovery of cardiac function in diabetic cardiomyopathy after replenishment of local vascular endothelial growth factor. Circulation 2005;111:2073–2085
55. Goldstein RE, Wasserman DH, McGuinness OP, Lacy DB, Cherrington AD, Abumrad NN. Effects of chronic elevation in plasma cortisol on hepatic carbohydrate metabolism. Am J Physiol 1993;264:E119–E127
56. Gudbjörnsdóttir S, Sjöstrand M, Strindberg L, Lönnroth P. Decreased muscle capillary permeability surface area in type 2 diabetic subjects. J Clin Endocrinol Metab 2005;90:1078–1082